# Thermodynamic equilibrium, kinetics, activation barriers, and reaction mechanisms for chemical reactions in Karst Terrains

W. B. White

**Abstract** Chemical reactions pertinent to karst systems divide broadly into (a) speciation reactions within aqueous solutions, (b) dissolution/precipitation and other acid/base reactions between aqueous solutions and solid minerals, and (c) redox reactions involving various carbon and sulfur-bearing species. As a backdrop against which other chemistry can be evaluated, selected phase diagrams and equilibrium speciation diagrams were calculated for the system Ca—Mg—O—H—C—S. The kinetics of reactions within this system span time scales from milliseconds for homogeneous reactions in solution through hundreds of hours for carbonate mineral dissolution reactions, to geologic time scales for reactions such as the aragonite/calcite inversion or the oxidation/reduction of native sulfur. In purely inorganic systems, kinetic barriers, typically on the order of tens of kJ/mole, are set by nucleation processes and by activated complex formation. Biological processes impact the purely inorganic chemistry by the following mechanisms: (a) Secretions and waste products from biological activity or consumption of $CO_2$ by organisms changes the chemistry in the microenvironments of reaction surfaces. Oxidation potentials, pH, and ion activities may be modified, thus shifting equilibria. (b) Reaction rates may be increased due to modification of activated complexes and thus the activation barriers to reaction. (c) Organic compounds or microorganisms may act as substrates, thus lowering nucleation barriers. The preservation of microorganisms in cave deposits does not necessarily prove a cause and effect relationship.

**Key words** Karst systems · Chemical reactions · Aqueous solutions · Carbonate mineral dissolution reactions · Kinetics · Thermodynamic equilibrium

Received: 21 December 1995 · Accepted: 9 January 1996

W. B. White
Department of Geosciences and Materials Research Laboratory, The Pennsylvania State University, University Park, PA 16802, USA

Paper presented at the conference "Breakthroughs in Karst Geomicrobiology and Redox Geochemistry", Colorado Springs, Colo., February, 1994

## Introduction

Caves are environments for a great variety of chemical reactions which mostly take place under conditions of temperature, $CO_2$ pressure, water vapor pressure, oxygen partial pressure, and chemical composition of aqueous solutions that maintain fixed patterns over periods of time measured in centuries or millennia. The chemistry is mostly inorganic chemistry and fairly simple organic chemistry. The reactions can be broadly categorized as:

(i) Hydration/dehydration reactions
(ii) Acid/base reactions
(iii) Phase transitions
(iv) Dissolution/precipitation reactions
(v) Redox reactions

Thermodynamics provides a framework for determining which reactions will proceed and in which direction. For reactions involving phases of variable composition, thermodynamics gives solubility limits and partial pressures of coexistent gas phases as related information. Thermodynamics, as it is used in this paper, describes systems at equilibrium. Thermodynamics says nothing about how long it would take a system to reach the equilibrium states. Thermodynamic equilibrium describes the bottom of the energy well. Mostly, final equilibrium states are insensitive to minor impurities and to environmental perturbations such as the presence of microorganisms.

The rate, describing the time required for the system to progress from some initial condition to the final state of thermodynamic equilibrium, is the subject of chemical kinetics. Unlike the equilibrium state itself which is unique, there may be many pathways from initial states to the equilibrium state and there may be intermediate metastable states in which the system may reside for long periods of time. The rate at which the system approaches equilibrium may vary by many orders of magnitude along different reaction pathways. Along a particular pathway, rates are sensitive to impurities, particle sizes,

reaction interfaces, and quite possibly the presence of microorganisms.
The objective of the present paper is to set down the thermodynamic framework for selected reactions in karst systems and to review what, if anything, is known about the kinetics of these reactions. The examples are selected to illustrate the types of reactions listed above. In each case a possible role for microorganisms is assessed.

## Some thermodynamic concepts

Here follows a short reminder of the thermodynamic concepts that underlie all chemical mechanisms and which define the reference states against which all kinetic and microbiological mechanisms must be compared. The concepts begin with the Gibbs free energy, $G$, (Nordstrom and Munoz 1985; Anderson and Crerar 1993) defined as

$$G = E + PV - TS, \tag{1}$$

where $E$ is the internal energy of the system, $P$ is pressure, $V$ is volume, $T$ is absolute temperature and $S$ is entropy. Neither the internal energy scale nor the Gibbs free energy scale have a natural zero point. By definition, the elements in their stable forms at the specified temperature have their Gibbs free energies set equal to zero. What is observed in chemical reactions is the free energy change between reactants and products. Compounds which are stable with respect to spontaneous decomposition into their component elements have negative Gibbs free energies. The energy decrease observed when a compound is formed from its component elements is the Gibbs free energy of formation $\Delta G_f^0$. The energy is written as a delta term because it is measured with respect to the elemental standard state. The superscript indicates that the compounds are themselves in their standard states – pure crystalline compounds, pure liquids, or pure gases at unit pressure (1 atmosphere in older literature; 0.1 MPa in current usage. See Wagman and others 1982). In spontaneous reactions, reactant phases form product phases with lower free energies (Fig. 1). The difference in Gibbs free energy of formation between reactant phases and product phases is the Gibbs free energy of reaction, $\Delta G_R^0$, which is directly related to the equilibrium constant, $K$, for the reaction

$$\Delta G_R^0 = -RT \ln K, \tag{2}$$

where $R$ is the gas constant = 8.3143 J mol$^{-1}$ K$^{-1}$.
The product phases with the lowest Gibbs free energies are the most stable and represent the equilibrium state if all reactions went to completion. However, there are frequently other possible products which are metastable with respect the stable phases, meaning that they have a higher Gibbs free energy. Both stable, $R \rightarrow$S, and metastable $R \rightarrow M$ reactions can be written and equilibrium constants can be calculated. It violates no thermodynamic principles that metastable phases are frequently observed,

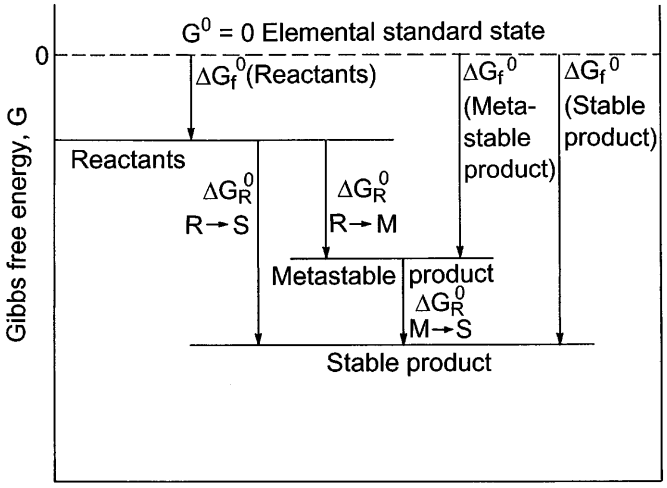


**Fig. 1**
Schematic diagram defining free energies of formation and free energies of reaction for stable and metastable reaction products

particularly in reactions near earth surface temperatures. The metastable phases are predicted to eventually decay to the stable phases, but "eventually" can be a very long time.
The reaction pathways followed in laboratory and natural systems are often determined by kinetics rather than by thermodynamics. How this works is illustrated schematically in Fig. 2. In order for the reactants to form the product phases, the system must cross an energy barrier, $\Delta E$. The energy barriers are determined by reaction mechanisms at the atomic scale. In the sketch given in Fig. 2, the reaction to the stable phase, $R \rightarrow S$, has a high energy barrier but the reaction to the metastable phase, $R \rightarrow M$, has a low energy barrier. Under these circumstances, the system will react to the metastable product in spite of a substantial energy benefit if it reacted to the stable product.
Whether the metastable product survives depends in turn on the activation barrier for the $M \rightarrow S$ reaction. Two possibilities are shown in Fig. 2. If the activation barrier is high, the metastable phase will persist indefinitely. If the barrier is lower, the metastable product will be observed to eventually decay to the stable phase.
Rates of reaction rise exponentially with increasing temperature, as described by the Arrhenius equation which ties the temperature dependence of the rates to the height of the activation barrier:

$$k = A_0 \exp(-\Delta E/RT). \tag{3}$$

For this reason, reactions at high temperatures generally proceed all the way to the final stable equilibrium state, while reactions at earth surface or cave temperatures hang up on metastable states more often than not. Details of reaction pathways are very sensitive to reaction mechanisms and to catalysts – inorganic, organic, or biological – that modify the energy barriers.

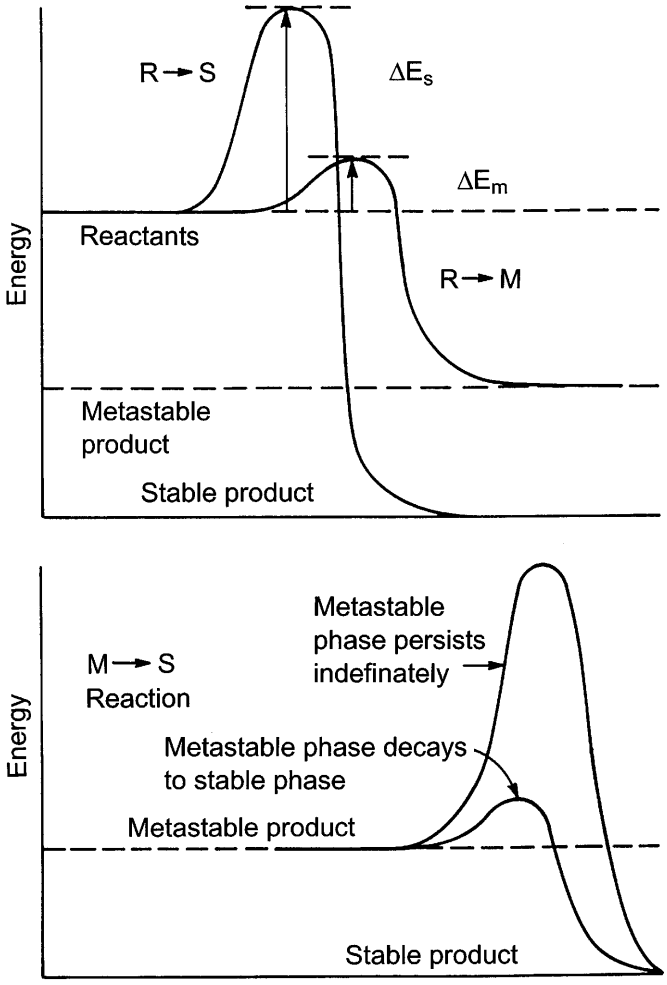


**Fig. 2**
Schematic diagrams showing activation barriers to energy flow from reactant phases to product phases

## Equilibria and kinetics in non-redox systems

The objective of this section is to illustrate several types of reactions that take place in the cave environment and to suggest ways in which these reactions might be modified by microorganisms.

### Hydration/dehydration reactions: the $MgSO_4-H_2O$ and $Na_2SO_4-H_2O$ systems

Mirabilite, $Na_2SO_4 \cdot 10H_2O$, and epsomite, $MgSO_4 \cdot 7H_2O$ are two hydrated sulfate salts that occur, sometimes as massive crystals, in dry caves. Mirabilite dehydrates completely in one step to thenardite, $Na_2SO_4-V$.

$$Na_2SO_4 \cdot 10H_2O \rightarrow Na_2SO_4 + 10\ H_2O$$

In equilibrium with liquid water at cave temperatures, mirabilite is the stable phase. As a crystalline phase in the cave atmosphere, however, there will be a certain water vapor partial pressure (or relative humidity) at which mirabilite and thenardite will coexist. Higher water vapor pressures will stabilize the mirabilite phase. Lower water vapor pressures will cause the mineral to dehydrate to thenardite.

$$P_{H_2O} = K_{mir}^{1/10} \quad (4)$$

The equilibrium constant varies with temperatures, so that the dependence of the dehydration curve can be calculated or can be determined experimentally as Hamad (1976) has done (Fig. 3).
The dehydration of epsomite, $MgSO_4 \cdot 7H_2O$, takes place in a series of steps of which the first

$$MgSO_4 \cdot 7H_2O \rightarrow MgSO_4 \cdot 6H_2O + H_2O$$

is most relevant to the cave environment. The water vapor partial pressure at which epsomite dehydrates to hexahydrite was determined experimentally (Kohler and Zaske 1964) to be

$$\log P_{H_2O} = -3207/T + 11.82, \quad (5)$$

and their result is also plotted on Fig. 3 along with the vapor pressure curve for pure water.
Both of these hydration/dehydration reactions are fast. The measured characteristic time (the inverse of the reaction rate constant) is 6.4 min for the epsomite/hexahydrite reaction (Hamad 1975). The rate for the dehydration of mirabilite is similar. Specimens of the mineral removed from the damp cave atmosphere (85% relative humidity where the crystals grew), decomposed and crumbled into a white powder, analyzed to be thenardite, in a

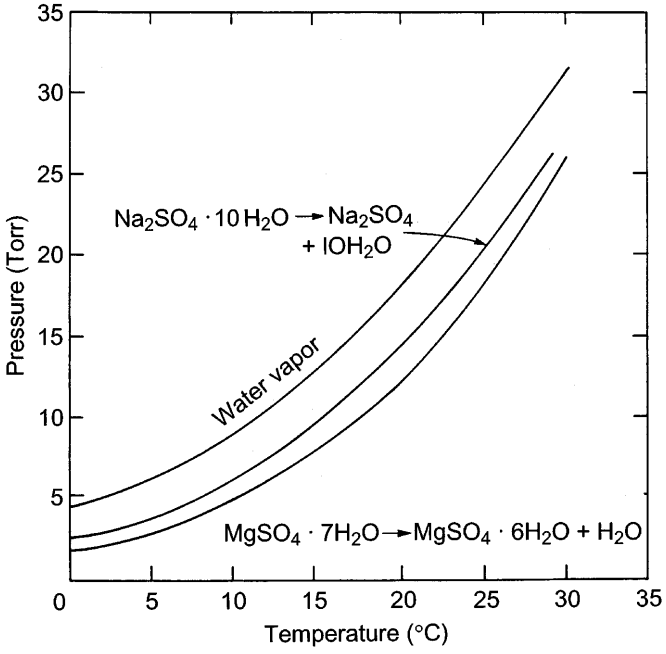


**Fig. 3**
Vapor pressure curves for dehydration of mirabilite to thenardite (based on data of Hamad 1976) and for dehydration of epsomite to hexahydrite (plotting equation of Kohler and Zaske 1964). Water vapor pressure curve is plotted from data in Handbook of Chemisty and Physics

matter of a few minutes. Both reactions can be reversed and both can be easily duplicated in the laboratory. It appears that the hydration/dehydration class of reactions in the cave environment can be accounted for by purely inorganic mechanisms.

### Homogeneous acid-base reactions: carbonic acid

An essential part of karst chemistry is the dissociation of carbonic acid which takes place in two steps.

$$H_2CO_3 \rightarrow H^+ + HCO_3^-,$$
$$HCO_3^- \rightarrow H^+ + CO_3^{-2}.$$

These reactions have been studied for many years and their equilibrium constants are well established (Plummer and Busenberg 1982; White 1988).
The reactions are very fast with characteristic time constants of a few milliseconds. Ionization reactions in homogeneous solutions mark the lower limit of the characteristic time scales in karst water kinetics. In most geochemical modelling of karst systems, these reactions are taken to be always at equilibrium.

### Heterogeneous acid-base reactions: the system $MgO-CO_2-H_2O$

The compositions of a set of hydrated and hydroxylated magnesium carbonates relevant to the cave environment are plotted in Fig. 4. Magnesite, $MgCO_3$, and nesquehonite, $MgCO_3 \cdot 3H_2O$ have been found rarely in caves. The most common hydrated magnesium carbonate is hydromagnesite. The other phases have not been reported from caves (Hill and Forti 1986). All of the magnesium carbonate minerals occur typically as white pasty masses known as moonmilk. Moonmilk is a speleothem term and includes all minerals including calcite and huntite that occur in pasty, chalky, microcrystalline form. Bacteria and algae have been found in moonmilks (Williams 1959; Cubbon 1976) which, along with the unusual morphology of the speleothems, has lead to the hypothesis that moonmilks are a result of the action of microorganisms.
The task at hand is to determine the thermodynamic stability of the various phases plotted in Fig. 4 and to see if the thermodynamic relations will rationalize the mineral occurrences observed. Although straightforward in principle, very high quality Gibbs free energies of formation are necessary. Langmuir (1965) calculated a temperature/$P_{CO_2}$ diagram for the phases in equilibrium with liquid water. Using one set of thermodynamic data, magnesite was predicted to be the only stable phase. Using different values for the Gibbs free energy of magnesite led to a diagram with nesquehonite as the stable phase under typical cave environmental conditions.
However, most moonmilks occur as loose masses on cave floors or as small blobs attached to other speleothems, not in contact with liquid water. Solid-vapor rather than solid-liquid reactions seem more pertinent. Of the phases represented in Fig. 4, artinite appears to be metastable and little is known of dypingite, so these phases cannot be included in the calculations. The system variables are temperature, water vapor partial pressure, and $CO_2$ partial pressures. The procedure is to write chemical reactions connecting the various minerals, write equations for the equilibria, calculate the equilibrium constants from thermodynamic data (Wagman and others 1982) using Eq. (2), and then plot the results on a log-log diagram (Fig. 5) with temperature held constant.

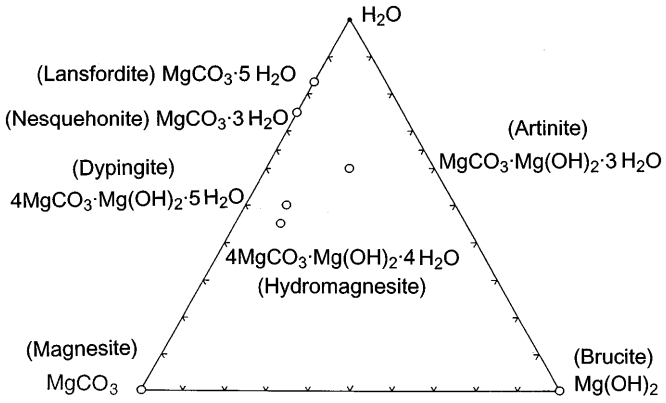


**Fig. 4**
Compositions of the known minerals in the ternary system $MgCO_3-Mg(OH)_2-H_2O$

Brucite is stable at very low $CO_2$ partial pressures, but as $CO_2$ pressure increases, brucite will react with $CO_2$ to form magnesite.

a. $Mg(OH)_2 + CO_2 \rightarrow MgCO_3 + H_2O.$

If water is present only in the vapor form, the equilibrium expression is

$$P_{H_2O}/P_{CO_2} = K_a = 10^{2.243} \quad (6)$$

On a log-log plot, Eq. (6) gives the brucite/magnesite phase boundary shown on Fig. 5.

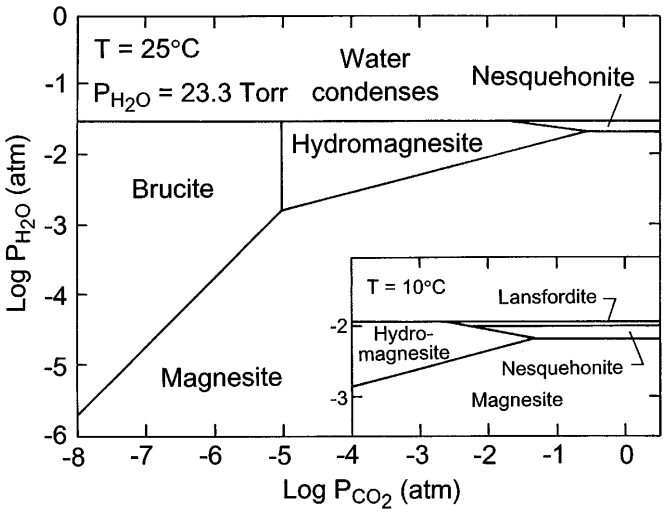


**Fig. 5**
Phase diagram for the system $MgO-CO_2-H_2O$ in the solid-vapor region. Each solid phase coexists with a vapor phase with varying water vapor and carbon dioxide partial pressure. Main diagram is isothermal at 25 °C; insert shows a portion of the diagram calculated at 10 °C

Under high water vapor partial pressures, increasing the $CO_2$ pressure converts brucite to hydromagnesite directly.

b. $4Mg(OH)_2 + 3CO_2 \rightarrow 3MgCO_3 \cdot Mg(OH)_2 \cdot 3H_2O$

The water content is the same on both sides of the equation, so this reaction is only a function of the $CO_2$ pressure. Note that the composition of hydromagnesite as written above is different by one mole of water from the formula in Fig. 4. There has been disagreement over the exact composition of this phase, and although the $4H_2O$ composition is now generally accepted, the thermodynamic data were constructed using the $3H_2O$ composition which must be retained for internal consistency in the calculations.

$$1/P_{CO_2}^3 = K_b = 10^{-15.099}. \quad (7)$$

The brucite/hydromagnesite phase boundary is a vertical line cut off at the high water vapor pressure end when $P_{H_2O}$ reaches the vapor pressure of liquid water.
At higher $CO_2$ pressures, hydromagnesite can be dehydrated to form magnesite.

c. $3MgCO_3 \cdot Mg(OH)_2 \cdot 3H_2O + CO_2 \rightarrow 4MgCO_3 + 4H_2O$

$$P_{H_2O}^4 / P_{CO_2} = K_c = 10^{-6.127}. \quad (8)$$

The hydromagnesite/magnesite phase boundary is required to meet the brucite/hydromagnesite and brucite/magnesite boundaries at a common point. The fact that it does is evidence for the internal consistency of the calculations.
Nesquehonite appears as a stable phase only at high $CO_2$ pressures. It is formed from hydromagnesite when the $CO_2$ pressure becomes sufficiently high to cause a replacement of the hydroxy groups in hydromagnesite.

d. $3MgCO_3 \cdot Mg(OH)_2 \cdot 3H_2O + CO_2 + 8H_2O \rightarrow 4MgCO_3 \cdot 3H_2O$

$$\frac{1}{(P_{CO_2} P_{H_2O}^8)} = K_d = 10^{13.694}. \quad (9)$$

Nesquehonite can also be formed by the direct hydration of magnesite.

e. $MgCO_3 \cdot 3H_2O \rightarrow MgCO_3 + 3H_2O$

$$P_{H_2O}^3 = K_e = 10^{-4.955}. \quad (10)$$

This reaction does not involve $CO_2$ exchange, and so plots as a horizontal line on Fig. 5. The nesquehonite/magnesite, hydromagnesite/nesquehonite, and hydromagnesite/magnesite boundaries must also meet at a common point.
Finally, there is the lansfordite phase. Lansfordite can dehydrate to form nesquehonite.

f. $MgCO_3 \cdot 5H_2O \rightarrow MgCO_3 \cdot 3H_2O + 2H_2O$

$$P_{H_2O}^2 = K_f = 10^{-2.795}. \quad (11)$$

At 25 °C, the lansfordite/nesquehonite boundary plots as a horizontal straight line located at $\log P_{H_2O} = -1.398$ which lies above the condensation line for liquid water. At 25 °C, lansfordite does not appear as a phase in equilibrium only with the cave atmosphere. Adjusting the various thermodynamic data to 10 °C, which can be done only roughly with the quantity and quality of data available, leads to the phase relations shown in the insert on Fig. 5. A narrow field for lansfordite appears just below the water condensation line. This is consistent with Langmuir's (1965) phase diagram for magnesium carbonates in equilibrium with liquid water. He shows the dehydration of lansfordite to nesquehonite occurring at 10 °C. Lansfordite has not been confirmed from a cave locality, but Harmon and others (1983) report some evidence for it in Castleguard Cave which lies beneath the Columbia Ice Field in Banff National Park, Alberta. The cave temperature varies from 1 to 3 °C. Samples collected from cold caves would need to be transported to the laboratory under refrigeration for lansfordite to survive until analysis.
The mineral stability diagram constructed in Fig. 5 rationalizes very well the mineral occurrences observed. In the cave environment, water vapor partial pressures are close to the condensation line and $CO_2$ partial pressures range from $10^{-3.5}$ to $10^{-2}$. The cave environment lies mainly in the hydromagnesite field and hydromagnesite is the magnesium carbonate mineral most commonly observed. Nesquehonite and magnesite occur occasionally, under rather exceptional conditions.
Is there a role for microorganisms as Williams (1959) and other workers have suggested? The kinetics of magnesium carbonate deposition reactions are unknown, so modifications of reaction rates are a potential role for microorganisms. However, no special mechanisms, inorganic, organic, or biological, need be invoked to explain mineral stability. The possibility must be entertained that the bacteria and algae observed in moonmilk deposits are there because these deposits form a favorable habitat for the organisms. The occurrence of microorganisms in cave mineral deposits is not, in itself, conclusive evidence that the microorganisms were necessary for the formation of the deposits.

### Phase transitions: the argonite/calcite inversion

Calcite, the trigonal polymorph of $CaCO_3$, and aragonite, the orthorhombic polymorph, are common cave minerals. Calcite is the thermodynamically stable phase under cave conditions. The large number of experimental investigations of the calcite/aragonite phase transition agree generally (Fig. 6) that aragonite becomes stable only at pressures above 300–500 MPa. The boundary line between the two thermodynamic stability fields extrapolates to 0.1 MPa at temperatures below absolute zero, thus proving that aragonite is everywhere metastable at atmospheric pressure. The mechanisms that allow the metastable deposition of aragonite in low pressure environments is the subject of a large literature (Carlson 1983). Regardless of how it formed, aragonite exists in caves in a metastable state and there is a thermodynamic driving force to convert it to the stable calcite (as shown schematically in Fig. 1). The kinetics of the aragonite/calcite inversion are a good illustration of the experimental difficulty in a laboratory setting and the interpretative difficulty in a field setting for understanding the controlling factors.

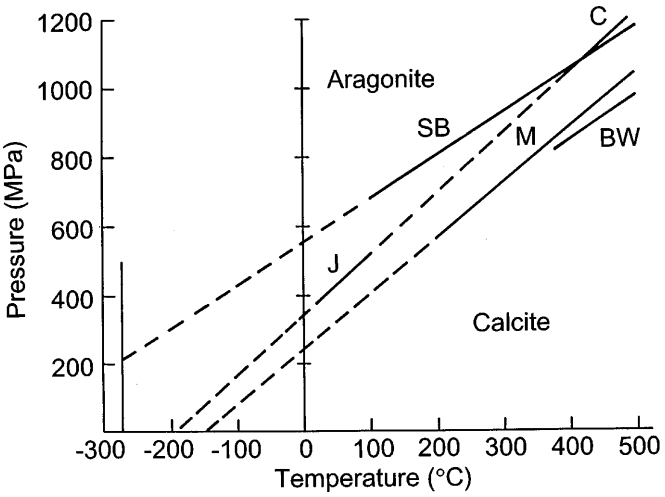


**Fig. 6**
Equilibrium *P-T* phase boundaries for calcite/aragonite phase transition. *SB*: Simmons and Bell (1963); *J*: Jamieson (1953); *M*: MacDonald (1956); *BW*: Boettcher and Wyllie (1968); *C*: Clark (1957)

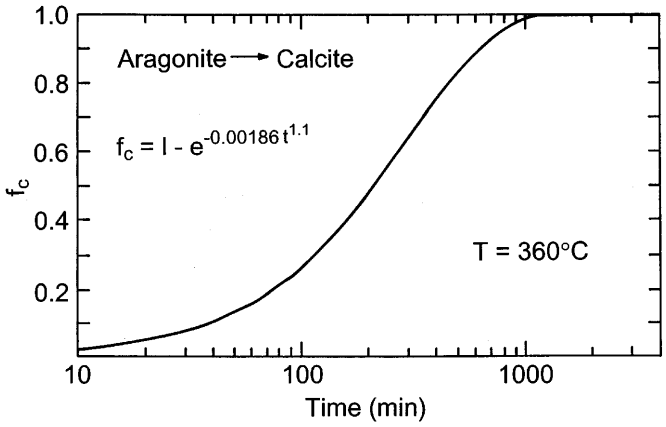


**Fig. 7**
Avrami equation for the solid-state conversion of aragonite to calcite fitted to the data of Kunzler and Goodell (1970). Aragonite from Lamb's Lair Cave, England. Temperature of experiments = 360 °C

The direct conversion of aragonite to calcite by solid-state reaction is extremely sluggish at earth surface temperatures and can be investigated experimentally only at temperatures in the range of 350–500 °C. A variety of rate equations have been proposed (Brar and Schloessin 1979) and the mechanism of transformation has been investigated in some detail (Liu and Yund 1993). Most useful is an Avrami-type equation of the form

$$f_c = 1 - \exp(-k t^n), \tag{12}$$

where $f_c$ is the fraction of the aragonite converted to calcite, $k$ is a rate constant and $n$ is an empirical exponent. Kunzler and Goodell (1970) measured the inversion kinetics of biogenic aragonite, precipitated aragonite, and one cave aragonite. The inversion curve for the cave aragonite was fitted to an Avrami equation (Fig. 7). The initial slow reaction results from the slow calcite nucleation rate within the aragonite specimen. As the number of available nuclei increases, the rate increases rapidly, reaching a maximum at some characteristic time given by the inflection point of the curve. As time passes, the available aragonite in the sample is gradually depleted and the rate slows down until at last conversion becomes complete. Data for the dry solid-solid transformation collected at several hundred degrees Celsius generally show an Arrhenius-type behavior [Eq. (3)] and yield the activation energies shown in Table 1. However, when the rates obtained in the laboratory at high temperatures are extrapolated to the typical cave temperature of 10 °C, reaction times are found to range from $10^{15}$ to $10^{45}$ years. Dry aragonite, in a dry cave passage, although thermodynamically metastable, is kinetically stable indefinitely.

Aragonite, however, does not persist indefinitely in the cave environment. There occur clusters of radiating crystals with the characteristic morphology of aragonite, which have partly or completely inverted to calcite (White 1994). Some alternative reaction pathway is needed to shift the aragonite/calcite phase transition across the high activation barrier. This is provided by a dissolution-reprecipitation mechanism. Aragonite, as a metastable phase, is more soluble than calcite. Aragonite can dissolve in the minute amounts of water present in damp caves and then reprecipitate as the less soluble calcite. Laboratory experiments in wet systems such as those of Bischoff and Fyfe (1968) and Bischoff (1969) lead to a different form of rate equation in which the fraction converted is given by the equation

$$f_c = k_T [Ca^{2+}] [HCO_3^-] t^2, \tag{13}$$

where $f_c$ is expressed in percent, $t$ is in hours, and the rate constant $k_T = 344$. Substitution of typical values for the calcium and bicarbonate concentrations for cave drip waters leads to 200 h as the time for 50% conversion at 10 °C. Although the mathematical form of the equation is clearly incorrect at long times, it provides a fit to the data that are in startling contrast to the measurements

**Table 1**
Activation energies for the aragonite-to-calcite transformation

| Experiment | *E*a (kJ/mole) | Source |
|---|---|---|
| Solid-solid conversion of metamorphic aragonite | 439 | Calculated from data of Brown, Fyfe and Turner (1962) |
| Solid-solid conversion of single crystal aragonite | 444 | Davis and Adams (1965) |
| Conversion of cave aragonite | 184 | Calculated from data of Kunzler and Goodell (1970) |
| Conversion in aqueous solution of precipitated aragonite | 240 | Bischoff (1969) |

on dry systems. The activation energy for the dissolution/reprecipitation reaction is about half that of the activation energy from the solid/solid conversion mechanism (Table 1).

Most natural environments in caves and shallow sedimentary systems are wet, but the laboratory conversion times are embarrassingly short. Aragonite/calcite transformation times observed in aragonite-depositing corals are on the order of a million years ("Pleistocene" according to Siegel 1960). Laboratory rates are much too fast compared with field observations and some inhibition mechanism is required to slow down the conversion. There is some evidence that minor concentrations of $Sr^{2+}$ provide the necessary inhibition (Siegel 1960; White 1994).

The contrast between dry reaction rates and wet reaction rates adjusted to a common temperature is at least 17 orders of magnitude. The comparison is between conversion times orders of magnitude greater than the age of the universe with conversion times that are geologically instantaneous. The well-studied calcite/aragonite system provides one of the most dramatic demonstrations of the importance of reaction mechanism in determining reaction kineties. It further illustrates the difficulty in separating catalytic effects due to microorganisms from catalytic effects from purely inorganic mechanisms.

### Calcite dissolution and precipitation

The dissolution and precipitation of calcium carbonate in marine environments, in surface streams, and in caves is one of the most intensely studied aspects of aqueous geochemistry. The parameters for discussion are the calcium ion activity, the saturation index with respect to calcite, and the carbon dioxide partial pressure, all of which can be calculated from chemical analyses of carbonate waters (see White 1988, Chap. 5).

The rate of calcite dissolution and precipitation far from equilibrium can be described by the Plummer-Wigley-Parkhurst rate equation (Plummer and others 1978; Reddy and others 1981). Dissolution reactions slow down as the system approaches equilibrium and rates become sensitive to details of reaction surfaces and the presence of inhibitor ions. The precipitation of calcite requires a finite supersaturation because of activation barriers to calcite nucleation and crystal growth. It appears that a supersaturation of at least $SI_c = +0.5$ is needed to initiate calcite precipitation with values in the range of $SI_c = +1$ required for maximum precipitation rates (Dreybrodt and others 1992). It is in this near-equilibrium regime where the influence of microorganisms is most likely to be felt.

Carbon dioxide partial pressures in karst waters are nearly always bigher than the ambient $CO_2$ pressure of the atmosphere ($10^{-3.5}$ atm) or of typical cave atmospheres ($10^{-3}$–$10^{-2.5}$ atm). The driving mechanism for calcite precipitation is loss Of $CO_2$. Carbon dioxide may be lost to the atmosphere by purely physical means such as diffusion or agitation in riffles and waterfalls. Carbon dioxide may also be utilized by cyanobacteria and other organisms during photosynthesis and thus be lost to the water (Pentecost 1990), although this appears not to be the dominent mechanism (Pentecost 1994, 1995).

Some typical karst water chemistry is shown schematically in Fig. 8. The vertical scale is the saturation index, where the zero line divides the diagram into waters undersaturated with respect to calcite and waters which are supersaturated with respect to calcite. The kinetic thresholds for the slowing down of dissolution reactions ($SI_c = -0.3$) and for the onset of precipitation ($SI_c = +0.5$) are shown as dashed lines. Waters emerging into surface streams from springs or flowing in cave passages on a channel fill of clastic sediment have an essentially constant concentration of $Ca^{2+}$ ions until the onset of precipitation. With some manipulation of the defining equation for the saturation index, it can be shown that the relationship between saturation index, calcium ion activity, and carbon dioxide partial pressure is

$$SI_c = \log \frac{a_{Ca^{2+}}}{P_{CO_2}^{1/3}} \frac{2^{2/3} K_2^{1/3} \gamma_{HCO_3^-}^{2/3}}{K_1^{1/3} K_{CO_2}^{1/3} K_c^{1/3} \gamma_{Ca^{2+}}^{2/3}}, \quad (14)$$

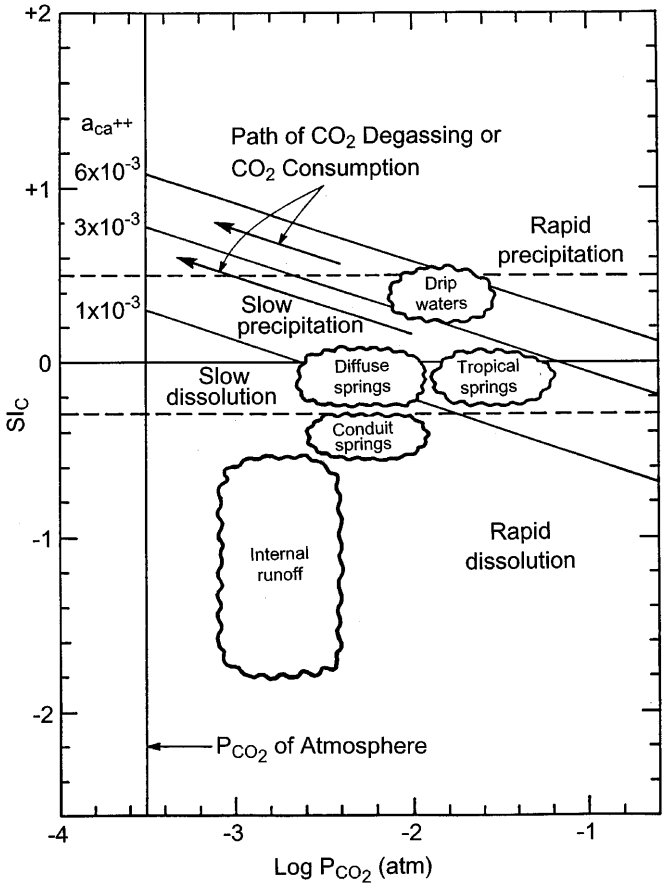


**Fig. 8**
Plot of calcite saturation index, $SI_c$, against $CO_2$ partial pressure calculated from water analyses. *Solid horizontal line* at $SI_c = 0$ describes waters exactly at equilibrium with calcite. *Horizontal dashed lines* indicate kinetic barriers for dissolution and precipitation. *Sloping lines* are contours of constant $Ca^{2+}$ activity as indicated. *Circled areas* indicate in a very schematic way the chemistry of the indicated types of water

where the *K*s and $\gamma$s are the usual equilibrium constants and activity coefficients. Lines of constant Ca-activity are plotted on Fig 8. The chosen values for Ca-activity contours correspond approximately to water hardnesses of 100, 300, and 600 mg/L and span the range of values usually observed in karst waters. Carbon dioxide loss will cause the system to follow a path parallel to the lines of constant calcium concentration, and if these paths reach the necessary supersaturation, calcite will precipitate and a travertine deposit will be formed.

Waters from sinkhole drains, shafts and other rapid inputs (called internal runoff in Fig. 8) are usually highly undersaturated. Loosing $CO_2$ down to the level of the atmospheric background will not cause these waters to supersaturate. Waters that percolate through $CO_2$-rich soil, then react with limestone at the soil/bedrock contact, and finally percolate downward to drip from cave roofs are usually rich in $CO_2$ and are near saturation or supersaturated. These are the waters that deposit stalactites, stalagmites, flowstone, and other speleothems in caves. $CO_2$ loss to the cave atmosphere drives these waters to supersaturation with concurrent deposition of calcite.

The most interesting case is that of surface waters that have emerged from springs. Three classes of springs are sketched in Fig. 8 to show general trends, although there would be considerable overlap if actual data were plotted. In temperate and northern climates, $CO_2$ partial pressures in spring waters usually fall in the range from $10^{-2}$ to $10^{-2.5}$. Those springs which drain from fracture aquifers are often near saturation, while those that drain from open conduits are undersaturated with saturation indices in the range from $-0.2$ to $-0.4$ or lower. In tropical and near-tropical climates, springs draining both fracture and conduit aquifers tend to be near saturation and also tend to have higher $CO_2$ partial pressures. Carbon dioxide loss at constant Ca-activity from tropical spring waters causes the chemistry to shift along the arrow shown in Fig. 8, so that the waters reach critical supersaturation for travertine deposition before the $CO_2$ partial pressure drops to the atmospheric background. Temperate climate springs, in contrast, can loose $CO_2$ down to the minimum set by the atmospheric background without reaching critical supersaturation for travertine deposition. The small slope of the arrow describing the chemical pathway for $CO_2$ degassing waters is determined by the dependence of saturation index on the inverse cube root of the $CO_2$ partial pressure (Eq. 14). This gives a relatively sensitive threshold for travertine deposition and may account for the observation that many spring-fed tropical streams contain travertine deposits while spring-fed temperate and northern streams rarely do.

Travertine-depositing springs and surface streams should be an excellent illustration of one mechanism for the influence of microorganisms, that in which the role of the organisms is to change the local geochemical environment. However, when the mechanism is worked out in detail, the $CO_2$ loss impacts the chemical system in exactly the same way, regardless of whether the loss is due to physical processes or due to consumption of $CO_2$ by cyanobacteria and other photosynthesis utilizing organisms. It is then very difficult to separate the physical and microbiological contributions to the total reaction. One of the best studied examples is Falling Spring Creek, Alleghany County, Virginia (Lorah and Herman 1988; Herman and Lorah 1988; Hoffer-French and Herman 1989). Although the appropriate organisms were present in large quantities in the massive travertine deposits (Pentecost 1990), the chemistry also can be interpreted on a strictly physical basis (Pentecost and Terry 1988).

An alternative role for microorganisms is to provide a nucleus on which calcite can precipitate as suggested by Ferris and others (1994). Reducing the nucleation barrier would appear on Fig. 8 as a lowering of the threshold supersaturation required for rapid precipitation. A careful comparison of supersaturation levels for surface travertines and cave travertines might help resolve this issue.

## Equilibria and kinetics in redox systems

### Redox equilibria for the system S—O—H

The S—O—H system is one of the most important in geochemistry. The pe-pH diagram for the S—O—H system appears in most geochemistry textbooks. What has been done here is to recalculate the equilibria using recent thermodynamic data (Wagman and others 1982) and to examine the specific conditions for elemental sulfur to coexist with gypsum.

Under oxidizing conditions, the stable species are the $HSO_4^-$ and $SO_4^{-2}$ ions. The second ionization constant of sulfuric acid is $1.015 \times 10^{-2}$, so that the bisulfate ion appears as a dominant species only below pH = 1.99. Under reducing conditions, $H_2S$ is the dominant species at low pH; the first ionization constant $= 1.018 \times 10^{-7}$, so that $HS^-$ becomes important in alkaline regimes. The second ionization constant of $H_2S$, as revised from Wagman and others' thermodynamic data, $= 1.215 \times 10^{-13}$. Only at pH > 12.9 does the fully ionized sulfide ion, $S^{-2}$, become dominant.

An important geochemical boundary is given by the oxidation/reduction reactions linking the reducing and oxidizing regions of the S—O—H system. In homogeneous solutions at low total sulfur activity, the following reactions must be considered:

a. $HSO_4^- + 8e^- + 9H^+ \rightarrow H_2S + 4H_2O$
$K = 4.143 \times 10^{38}$,
$pe = 4.827 - 9/8\ pH$; (15)

b. $SO_4^{-2} + 8e^- + 10H^+ \rightarrow H_2S + 4H_2O$
$K = 4.104 \times 10^{40}$,
$pe = 5.077 - 5/4\ pH$; (16)

c. $SO_4^{-2} + 8e^- + 9H^+ \rightarrow HS^- + 4H_2O$
$K = 2.393 \times 10^{34}$,
$pe = 4.203 - 9/8\ pH$. (17)

The ionization and redox reactions can be compiled into a revised pe-pH diagram (Fig. 9). The lines are speciation

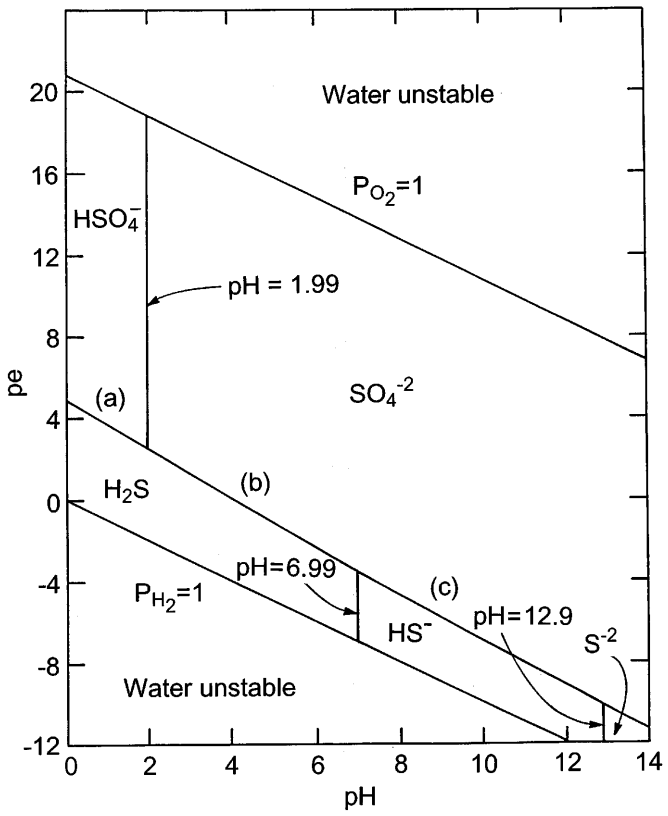


**Fig. 9**
Calculated speciation diagram for system S—O—H at total sulfur activity $<5\times10^{-6}$. *Labeling on speciation boundaries* refers to reactions given in the text. There are no solids in this diagram; *labeled fields* indicate dominant aqueous species

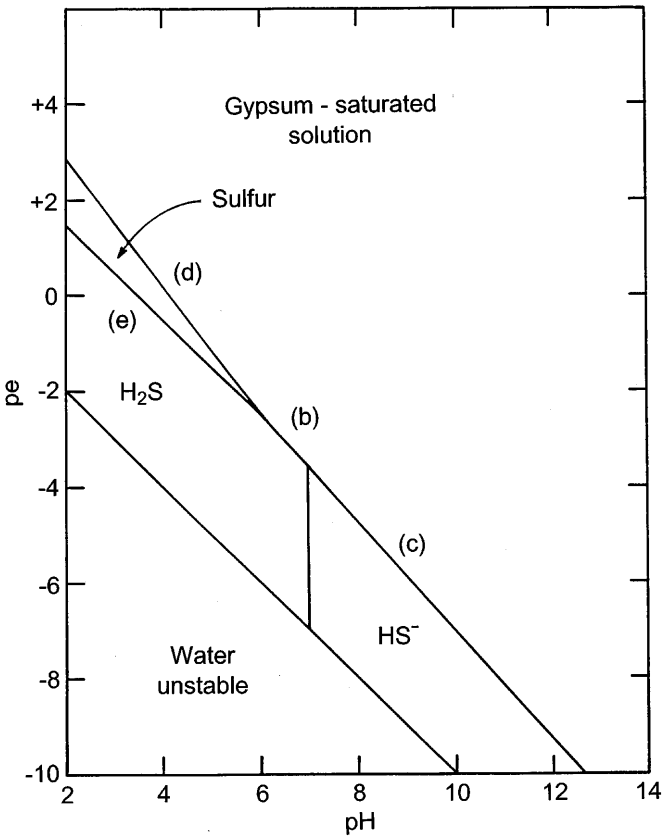


**Fig. 10**
Calculated phase and speciation diagram for system S—O—H with liquid in equilibrium with solid gypsum. The apex of the narrow triangle bounded by reactions (*b*), (*d*), and (*e*) marks the stability limit of solid elemental sulfur

boundaries obtained by setting equal the activities of species on opposite sides of the lines. This diagram applies to a homogeneous solution at 25 °C with total sulfur activity less than $5\times10^{-6}$.

As the total sulfur activity increases, a field of solid elementar sulfur appears at the low pH side of the diagram and extends to higher pH values as the sulfur activity increases. This gives rise to two additional reactions:

d. $SO_4^{-2}+6e^-+8H^+\rightarrow S^\circ+4H_2O$
$K=5.464\times10^{35}$,
$pe=5.956+1/6\log a_{SO_4}-4/3\ pH$; (18)

e. $S^\circ+2e^-+2H^+\rightarrow H_2S$
$K=7.511\times10^4$,
$pe=2.438-1/2\log a_{H_2S}-pH$. (19)

The sulfate activity reaches a limit when the solution becomes saturated with respect to gypsum. Gypsum solubility can be calculated:

$CaSO_4\cdot2H_2O\rightarrow Ca^{+2}+SO_4^{-2}+2H_2O$
$K_{gyp}=a_{Ca}a_{SO_4}=4.32\times10^{-5}$. (20).

By setting the activities of oxidized and reduced species equal to the activity of sulfate for gypsum saturation, $a_{SO_4}=6.57\times10^{-3}$, the diagram shown in Fig. 10 is obtained. The diagram shows the maximum extent of the field of elemental sulfur which terminates at pH = 6.19 for solutions saturated with gypsum.

Native sulfur appears as well-crystallized bulk deposits in association with gypsum in Cottonwood Cave, Carlsbad Caverns, and Lechuguilla Cave, Guadalupe Mountains, New Mexico (Davis 1973; Hill 1987). The coexistence of sulfur and gypsum defines an upper limit for the oxidation potential in the solutions from which the minerals were deposited. The current model for the origin of the caves of the Guadalupe mountains postulates a deep source of $H_2S$ in the petroleum-containing sediments of the Delaware Basin to the east. The caves are thought to be formed in the mixing zone where rising highly reducing sulfide-bearing waters meet descending oxygen-rich meteoric waters. Oxidation of $H_2S$ to elemental sulfur proceeds easily on a time scale of minutes to hours by purely inorganic mechanisms. The reduction of sulfate ion to elemental sulfur is much more sluggish and often occurs only in the presence of bacteriological catalysts. Hill (1987) found no evidence for bacterial action in the Carlsbad Caverns sulfur deposits. The solutions that formed these deposits no longer exist. Thermodynamic

arguments cannot resolve the question of whether sulfur deposition takes place by inorganic or microbiological processes. The calculations given above place limits on the chemistry of the solutions but are otherwise compatible with both mechanisms.

### Redox equilibria for the system Mn—O—C—H

The mobile species of manganese in the natural environment is the $Mn^{2+}$ ion and its hydroxy complexes. $Mn^{2+}$ is stable in acidic and reducing conditions. It readily oxidizes to the $Mn^{4+}$ which precipitates as one of the highly insoluble family of manganese dioxides. Black manganese oxides appear in marine and fresh water sediments, in wetlands, and as cave stream deposits. Black manganese oxides act as scavengers for other metals and manganese redox chemistry is closely tied to the geochemical and biogeochemical cycles of many elements (Burdige 1993). One analyzed cave sample of non-crystalline manganese oxide contained percent quantities of copper, zinc, nickel and cobalt (White and others 1985).

Manganese oxides occur in caves as black coatings on stream cobbles and more rarely as thick masses of material on cave floors. The deposits are poorly crystalline and most are amorphous to x-ray diffraction, making identification difficult. The few deposits that have been analyzed in detail contain birnessite, ideally $CaMn_6O_{13}\cdot 3H_2O$, as the dominant mineral (Moore 1981; Hill 1982; Chess, Scheetz and White, unpublished data). The Mn—O—H—C system illustrates very well an important pitfall in the application of thermodynamics to low-temperature systems. Free energies of formation are usually measured on well-crystallized solids of stoichiometric composition. The solid phases that precipitate from aqueous solutions are often extremely fine-grained, so that surface energy makes a significant contribution to the free energy. They are often poorly crystallized and often deviate from their ideal stoichiometry. The free energies of formation of the substances in the cave deposits are not the same as that listed in the thermodynamic tables.

There is a large literature on the Mn—O—H—C system and many Eh-pH and pe-pH diagrams have been published (e.g. Brenet and others 1963; Hem 1985; Brookins 1988). Calculation of a pe-pH diagram tailored to the cave environment has been attempted. The results are not as accurate as one might wish because of the absence of good thermodynamic data for the actual phases present in the cave deposits.

One of the most important of these reactions is the oxidation of the $Mn^{2+}$ ion to $MnO_2$.

$$Mn^{2+} + 2H_2O \leftrightarrow MnO_2 + 4H^+ + 2e^-,$$
$$pe = -1/2 \log K - 1/2 \log a_{Mn^{2+}} - 2\,pH. \quad (21)$$

As is customary, the activity of $Mn^{2+}$ was set equal to $10^{-6}$ molal which is about the limit of detection using ordinary methods of cation analysis. The relationship is then determined by the numerical value of $K$, which in turn depends on the choice of free energy of formation of $MnO_2$. Three possibilities are

$$pe = 23.68 - 2\,pH \quad \text{(pyrolusite?)}, \quad (22)$$
$$pe = 24.53 - 2\,pH \quad \text{(nsutite)}, \quad (23)$$
$$pe = 24.87 - 2\,pH \quad \text{(birnessite)}. \quad (24)$$

Equation 22 was based on the free energy of formation of $MnO_2$ given by Wagman and others (1982). The phase is not specified but is presumably pyrolusite, the stable, near-stoichiometric polymorph. Free energies for nsutite and birnessite were taken from Bricker (1965). The differences in the position of the oxidation boundary is more than an order of magnitude but not great in terms of the total variation of pe in aqueous systems. The birnessite line (Eq. 24) is plotted in Fig. 11. Bricker made his measurements on a birnessite-like phase called delta-$MnO_2$. The highly variable chemical composition and transition metal content of natural birnessites is very likely to shift the phase boundaries from those calculated from laboratory materials.

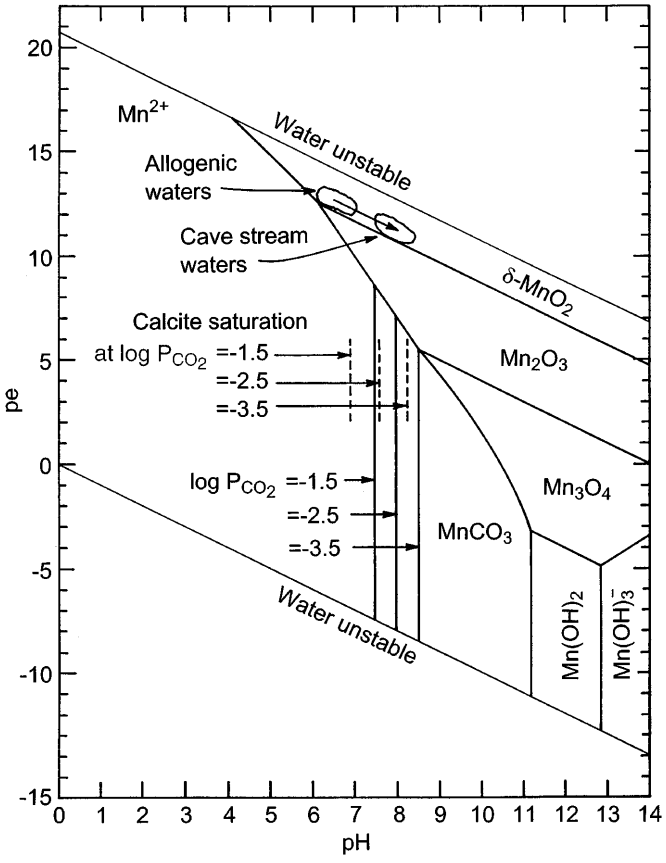


**Fig. 11**
pe-pH diagram for the system Mn—O—H—C. *Vertical lines* labeled with $CO_2$ pressures are solubility contours for $MnCO_3$ at the $CO_2$ pressures shown. *Parallel dashed lines* mark saturation of the solution with respect to calcite for the same $CO_2$ pressures. See text for details of calculations

The oxidation of $Mn^{2+}$ to bixbyite is also needed to construct the pe-pH diagram (Fig. 11). The reaction is

$$2\,Mn^{2+} + 3\,H_2O \leftrightarrow Mn_2O_3 + 6\,H^+ + 2\,e^-,$$
$$pe = -\log a_{Mn^{2+}} - 1/2 \log K - 3\ pH, \quad (25)$$

$$pe = 31.096 - 3\ pH. \quad (26)$$

There are a series of reduction reactions between the manganese oxides. The reduction of birnessite to bixbyite is described by the reaction

$$2\,MnO_2 + H^+ + 2\,e^- \leftrightarrow Mn_2O_3 + OH^-,$$
$$pe = 1/2\,[\log K - \log K_w] - pH. \quad (27)$$

Using the Bricker (1965) values of the free energy of birnessite and the Wagman and others (1982) values for the other species, $K = 1.955 \times 10^{23}$, giving the birnessite/bixbyite phase boundary as

$$pe = 18.646 - pH. \quad (28)$$

According to the Wagman and others (1982) thermodynamic data, bixbyite, $Mn_2O_3$, is the stable phase of $Mn^{3+}$ rather than manganite, MnOOH, as shown on some diagrams.

The reduction of bixbyite to hausmannite is described by the reaction

$$3\,Mn_2O_3 + H^+ + 2\,e^- \leftrightarrow 2\,Mn_3O_4 + OH^-,$$
$$pe = 1/2\,[\log K - \log K_w] - pH. \quad (29)$$

The equilibrium constant is $1.191 \times 10^{14}$, giving the bixbyite/hausmannite boundary as

$$pe = 14.038 - pH. \quad (30)$$

If the oxidation of $Mn^{2+}$ takes place in a carbonate environment as it certainly does in karst groundwater systems, then the precipitation and solubility of rhodochrosite, $MnCO_3$, must be taken into account. Because the hydrogen ion activity is taken as a system variable, the relevant reaction is

$$MnCO_3 + H^+ \leftrightarrow Mn^{2+} + HCO_3^-.$$

The karst system is also open to carbon dioxide, so that, with some manipulation, the pH for the $10^{-6}$ $Mn^{2+}$ activity contour can be calculated for various representative $CO_2$ pressures.

$$pH = 1/2$$
$$[-\log P_{CO_2} - \log a_{Mn^{2+}} - \log K_{CO_2} - \log K_1 + \log K_{rh}], \quad (31)$$

The equilibrium constant for the reaction given is calculated to be $K_{rh} = 0.478$. Solubility contours for $\log P_{CO_2} = -1.5,\ -2.5,\ -3.5$ are shown in Fig. 11. These span the range of $CO_2$ pressures that might be expected in karst waters.

Also shown in Fig. 11 by short dashed lines are the pH values at which the solution would be saturated with calcite for the same $CO_2$ pressures used to describe the rhodochrosite solubility. The lines all lie to the left of the rhodochrosite solubility lines, indicating that the system would be saturated with calcite at lower pH values than those that would cause rhodochrosite to precipitate.

Thus, in a karst environment sufficiently reducing to stabilize $Mn^{2+}$, the $Mn^{2+}$ ion could co-precipitate as a trace element in calcite rather than form a separate rhodochrosite phase.

The highly reducing, high pH corner of Fig. 11, involving equilibria between rhodochrosite, $MnCO_3$, hausmannite, $Mn_3O_4$, pyrochroite, $Mn(OH)_2$, and further dissolution due to the formation of hydroxy complexes at very high pH, was taken from the diagram published by Brookins (1988). There is a serious discrepancy in the Gibbs free energy of formation of $Mn(OH)_2$ (labeled as "amorphous") in the tables of Wagman and others (1982). There is further uncertainty about whether $Mn(OH)_2$ should appear as a solid phase at a maximum $Mn^{2+}$ activity of $10^{-6}$. According to the speciation diagram of Baes and Mesmer (1976), a $10^{-6}$ $Mn^{2+}$ solution is undersaturated with respect to $Mn(OH)_2$ and this field on the pe-pH diagram should be replaced with a solution in which the dominant species in $Mn_2(OH)_3^+$. Given the status of the fundamental data and also the lack of relevance to karst systems of this corner of the pe-pH diagram, no revised calculations were attempted.

Many cave streams that contain stream cobbles coated with black manganese oxides are derived from catchments underlain by non-carbonate rocks. These allogenic waters typically have pH values in the range of 6–7. When the waters enter the karst system, the pH rises, mostly due to reaction between dissolved $CO_2$ and the carbonate bedrock. Few Eh values have been measured on cave stream waters. Indeed, direct measurements might well be meaningless (see Lindberg and Runnells 1984) because of the low concentrations of redox ions. However, most surface streams and cave waters are well aerated and contain near-saturation values of dissolved oxygen. Thus, it can reasonably be expected that pe values will lie just below the upper water stability line. The expected chemistry is sketched in Fig. 11. The manganese-carrying allogenic waters are already close to or over the oxidation line when they enter the karst. Further increase in pH drives the water chemistry deeper into the birnessite field, where the dissolved $Mn^{2+}$ can oxidize to form the insoluble black oxide deposits.

The oxidation of $Mn^{2+}$ in cave waters to form coatings and deposits of birnessite and related $MnO_2$ minerals seems very likely to involve microorganisms as a catalyst. This is supported by evidence that $Mn^{2+}$ oxidizes in a matter of days in the presence of bacteria (Ehrlich 1968; Emerson and others 1982) but remains metastable for years in the absence of catalysts (Diem and Stumm 1984). Further evidence that more than inorganic processes are involved is provided by the distribution of observed manganese deposits in caves. Thick black coatings occur often on sandstone cobbles in stream beds and on chert beds exposed in the cave walls. It is much less common to find coatings on limestone blocks or on the limestone of the cave walls. Silica surfaces are clearly preferred over carbonate surfaces. The pronounced preference for substrate is a characteristic of control by biological mechanisms rather than a inorganic precipitation reaction.

## Conclusions

Examination of the thermodynamics of a selection of chemical reactions in cave environments leads to several conclusions, mostly tentative, about the interrelationships between the inorganic chemistry and the occurrence of microorganisms.

(a) The presence of microorganisms in a particular mineral deposit does not necessarily indicate a cause/effect relationship. As pointed out in the case of the magnesium carbonate minerals, these deposits may simply form a favorable substrate for bacterial and algal growth. Are the minerals there because of the microorganisms or are the microorganisms there because of the minerals?

(b) The rate-limiting mechanisms for many mineral precipitation reactions is the formation of initial nuclei of the product phases. If microorganisms form a suitable substrate for the growth of the mineral phases, particularly if there is an epitaxial relationship between the crystal structure of the mineral and the surface of the microorganism. The lowered nucleation barriers, by seeded or epitaxial growth, can greatly enhance rates of reaction and may also modify reaction pathways.

(c) Organisms modify microenvironments, thus changing reaction chemistry or appearing to shift phase boundaries. The consumption of $CO_2$ by cyanobacteria, thus lowering $CO_2$ pressures, increasing supersaturation, and enhancing precipitation rates of travertines, is a particularly good example.

(d) Organisms act as agents for electron transfer in redox reactions. This is the most frequently assigned role for microorganisms and it is seen in caves as sulfide/sulfur/sulfate reactions and in manganese deposition reactions. The role of microorganisms is catalytic. Microorganisms modify rates, not thermodynamics.

(e) Organisms can act as complexing agents, modifying activated intermediates, and thus lowering activation barriers. No definitive examples were found among the karst chemistry reactions examined.

## References


Anderson GM and Crerar DA (1993) Thermodynamics in Geochemistry. New York: Oxford University Press, 588 pp

Baes CF Jr and Mesmer RE (1976) The Hydrolysis of Cations. New York: Wylie, 490 pp

Bischoff JL (1969) Temperature controls on aragonite-calcite transformation in aqueous solution. Am Mineral 54:149–155

Bischoff JL and Fyfe WS (1968) Catalysis, inhibition, and the calcite-aragonite problem. I. The aragonite-calcite transformation. Am J Sci 266:65–79

Boettcher AL and Wyllie PJ (1968) The calcite-argonite transition measured in the system $CaO-CO_2-H_2O$. J Geol 76:314–330

Brar NS and Schloessin HH (1979) Effects of pressure, temperature, and grain size on the kinetics of the calcite → aragonite transformation. Can J Earth Sci 16:1402–1418

Brenet JP, Gabano JP, and Reynaud J (1963) Complements apportes au diagramme tension-pH du manganese. Electrochim Acta 8:207–216

Bricker OP (1965) Some stability relations in the system $Mn-O_2-H_2O$ at 25° and one atmosphere total pressure. Am Mineral 50:1296–1354

Brookins DG (1988) Eh-pH Diagrams for Geochemistry. Berlin: Springer, 176 pp

Brown WH, Fyfe WS, and Turner FJ (1962) Aragonite in California glaucophane schists and the kinetics of the aragonite-calcite transformation. J Petrol 3:566–582

Burdige DJ (1993) The biogeochemistry of manganese and iron reduction in marine sediments. Earth Sci Rev 35:249–284

Carlson WD (1983) The polymorphs of $CaCO_3$. In: Reeder RJ (Ed.) Carbonates: Mineralogy and Chemistry. Rev Mineral 11:191–225

Clark SP (1957) A note on calcite-aragonite equilibrium. Am Mineral 42:564–566

Cubbon BD (1976) Cave flora. Chapt. 11 in Ford TD and Cullingford CHD (Eds.) The Science of Speleology. London: Academic Press, 423–452

Davis DG (1973) Sulfur in Cottonwood Cave, Eddy County, New Mexico. Natl Speleol Soc Bull 35:89–95

Davis BL and Adams LH (1965) Kinetics of the calcite-aragonite transformation. J Geophys Res 70:433–441

Diem D and Stumm W (1984) Is dissolved $Mn^{2+}$ being oxidized by $O_2$ in absence of Mn-bacteria or surface catalysts? Geochim Cosmochim Acta 48:1571–1573

Dreybrodt W, Buhmann D, Michaelis J, and Usdowski E (1992) Geochemically controlled calcite precipitation by $CO_2$ outgassing: Field measurements of precipitation rates in comparison to theoretical predictions. Chem Geol 97:285–294

Ehrlich HL (1968) Bacteriology of manganese nodules II. Manganese oxidation by cell-free extract from a manganese nodule bacterium. Appl Microbiol 16:197–202

Emerson S, Kalhorn S, Jacobs L, Tebo BM, Nealson KH, and Rosson RA (1982) Environmental oxidation rate of manganese (II): bacterial catalysis. Geochim Cosmochim Acta 46:1073–1079

Ferris FG, Wiese RG, and Fyfe WS (1994) Precipitation of carbonate minerals by microorganisms: Implications for silicate weathering and global carbon dioxide budget. Geomicrobiol J 12:1–13

Hamad S El D (1975) An experimental study of the salt hydrate $MgSO_4 \cdot 7H_2O$. Thermochim Acta 13:409–418

Hamad S El D (1976) A study of the reaction $Na_2SO_4 \cdot 10H_2O \rightarrow Na_2SO_4 + 10H_2O$ in the temperature range 0 to 25 °C. Thermochim Acta 17:85–96

Harmon RS, Atkinson TC, and Atkinson JL (1983) The mineralogy of Castleguard Cave, Columbia Icefields, Alberta, Canada. Arctic Alpine Res 15:503–516

Hem JD (1985) Study and interpretation of the chemical characteristics of natural water. US Geol Survey Water-Supply Pap 2254, 263 pp

Herman JS and Lorah MM (1988) Calcite precipitation rates in the field: Measurement and prediction for a travertine-depositing stream. Geochim Cosmochim Acta 52:2347–2355

Hill CA (1982) Origin of black deposits in caves. Natl Speleol Soc Bull 44:15–19

Hill CA (1987) Geology of Carlsbad Cavern and other caves in the Guadalupe Mountains, New Mexico and Texas. New Mexico Bur Mines Bull 117, 150 pp

Hill CA and Forti P (1986) Cave Minerals of the World. Huntsville: Natl Speleological Soc, 238 pp

Hoffer-French KJ and Herman JS (1989) Evaluation of hydrological and biological influences on $CO_2$ fluxes from a karst stream. J Hydrol 108:189–212

Jamieson JC (1953) Phase equilibrium in the system calcite-aragonite. J Chem Phys 21:1385–1390
Kohler K and Zaske P (1964) Der thermische Abbau von $MgSO_4 \cdot 7H_2O$, $NiSO_4 \cdot 7H_2O$, $ZnSO_4 \cdot 7H_2O$. Zeits anorg allgem Chem 331:2–6
Kunzler RH and Goodell HG (1970) The aragonite-calcite transformation. A problem in the kinetics of a solid-solid reaction. Am J Sci 269:360–391
Langmuir D (1965) Stability of carbonates in the system $MgO-CO_2-H_2O$. J Geol 73:730–754
Lindberg RD and Runnells DD (1984) Ground water redox reactions: An analysis of equilibrium state applied to Eh measurements and geochemical modeling. Science 225:925–927
Liu M and Yund RA (1993) Transformation kinetics of polycrystalline aragonite to calcite: new experimental data, modelling, and implications. Contrib Mineral Petrol 114:465–478
Lorah MM and Herman JS (1988) The chemical evolution of a travertine-depositing stream: Geochemical processes and mass transfer reactions. Water Resour Res 24:1541–1552
MacDonald GJF (1956) Experimental determination of calcite-aragonite equilibrium relations at elevated temperatures and pressures. Am Mineral 41:744–756
Moore GW (1981) Manganese deposition in limestone caves. Proc. 8th Internatl. Congress Speleology, Bowling Green, KY, pp 642–644
Nordstrom DK and Munoz JL (1985) Geochemical Thermodynamics. Benjamin/Cummings Publishing Co., Menlo Park, CA 477 pp
Pentecost A (1990) The algal flora of travertine: An overview. In: Travertine-Marl: Stream Deposits in Virginia. Herman JS and Hubbard DA Jr., Eds. VA Div Mineral Resour Publ 101:117–127
Pentecost A (1994) Formation of laminate travertines at Bagno Vignone, Italy. Geomicrobiol J 12:239–251
Pentecost A (1995) Geochemistry of carbon dioxide in six travertine depositing waters of Italy. J Hydrol 167:263–278
Pentecost A and Terry C (1988) Inability to demonstrate calcite precipitation by bacterial isolates from travertine. Geomicrobiol J 6:185–194
Plummer LN and Busenberg E (1982) The solubilities of calcite, aragonite, and vaterite in $CO_2-H_2O$ solutions between 0 and 90 °C, and an evaluation of the aqueous model for the system $CaCO_3-CO_2-H_2O$. Geochim Cosmochim Acta 46:1011–1040
Plummer LN, Wigley TML, and Parkhurst DL (1978) The kinetics of calcite dissolution in $CO_2$-water systems at 5° to 60 °C and 0.0 to 1.0 atm $CO_2$. Am J Sci 278:179–216
Reddy MM, Plummer LN, and Busenberg E (1981) Crystal growth of calcite from calcium bicarbonate solutions at constant $P_{CO_2}$ and 25 °C: A test of a calcite dissolution model. Geochim Cosmochim Acta 45:1281–1289
Siegel FR (1960) The effect of strontium on the aragonite-calcite ratios of Pleistocene corals. J Sediment Petrol 30:297–304
Simmons G and Bell P (1963) Calcite-aragonite equilibrium. Science 139:1197–1198
Wagman DD, Evans WH, Parker VB, Schumm RH, Halow I, Bailey SM, Churney KL, and Nuttall RL (1982) The NBS tables of chemical thermodynamic properties. J Phys Chem Ref Data, 11, suppl 2, 392 pp
White WB, Scheetz BE, Atkinson SD, Ibberson D, and Chess CA (1985) Mineralogy of Rohrer's Cave, Lancaster County, Pennsylvania. Natl Speleol Soc Bull 47:17–27
White WB (1988) Geomorphology and Hydrology of Karst Terrains. New York: Oxford University Press, 464 pp
White WB (1994) The anthodites from Skyline Caverns, Virginia: The type locality. Bull Natl Speleol Soc 56:23–26
Williams AM (1959) The formation and deposition of moonmilk. Trans Cave Res Group Great Britain 5:135–138